We are IntechOpen,
the world's leading publisher of
Open Access books
Built by scientists, for scientists

4,800
Open access books available

122,000
International authors and editors

135M
Downloads

Our authors are among the

154
Countries delivered to

TOP 1%
most cited scientists

12.2%
Contributors from top 500 universities

BOOK
CITATION
INDEX
CLARIVATE ANALYTICS
INDEXED

WEB OF SCIENCE™

Selection of our books indexed in the Book Citation Index
in Web of Science™ Core Collection (BKCI)

Interested in publishing with us?
Contact book.department@intechopen.com

Numbers displayed above are based on latest data collected.
For more information visit www.intechopen.com

Direct Electron Transfer of Human Hemoglobin Molecules on Glass/Tin-Doped Indium Oxide

Flavio Dolores Martínez-Mancera and
José Luis Hernández-López

Additional information is available at the end of the chapter

Abstract

Interfacial electron transfer kinetics of the *haem* (Fe^{III}/Fe^{II}) group in human hemoglobin molecules were investigated on glass/tin-doped indium oxide electrodes. Factors such as surface roughness, crystallinity, hydrophilicity and partial polarization of the working electrode played an important role to provide a more compatible microenvironment for protein adsorption. Results suggested that direct electron transfer from electrode to *haem* (Fe^{III})-H_2O intermediate is coupled to proton at near physiological pH ($I = 0.035$, $pH = 7.2$).

Keywords: cyclic voltammetry, direct-electron-transfer, human hemoglobin, tin-doped indium oxide electrode, surface electron transfer rate constant

1. Introduction

Haem-containing proteins such as hemoglobin (Hb), also spelled haemoglobin, are macromolecules that consist in an assembly of four globular polypeptide chains, tightly associated with a nonprotein *haem* group by means a complex arrangement folding pattern (α-helix). The *haem* group consists of an iron atom chelated to a porphyrin ring (*cf.* **Figure 1**), which allow to carry the oxygen in the red blood cells to whole body of all vertebrates as well as some invertebrates. Although the iron atom can take any of its oxidation states (Fe^{II} or Fe^{III}), the ferrihemoglobin (methemoglobin, metHb) (Fe^{III}) cannot bind oxygen [1]. In adult humans, the most common Hb type is a tetramer well-known as Hb A, consisting of two α and two β subunits noncovalently bound ($\alpha_2\beta_2$). These subunits are structurally similar to themselves and about the same molecular size. The total molecular weight of the Hb A is *ca*. 64 kDa.
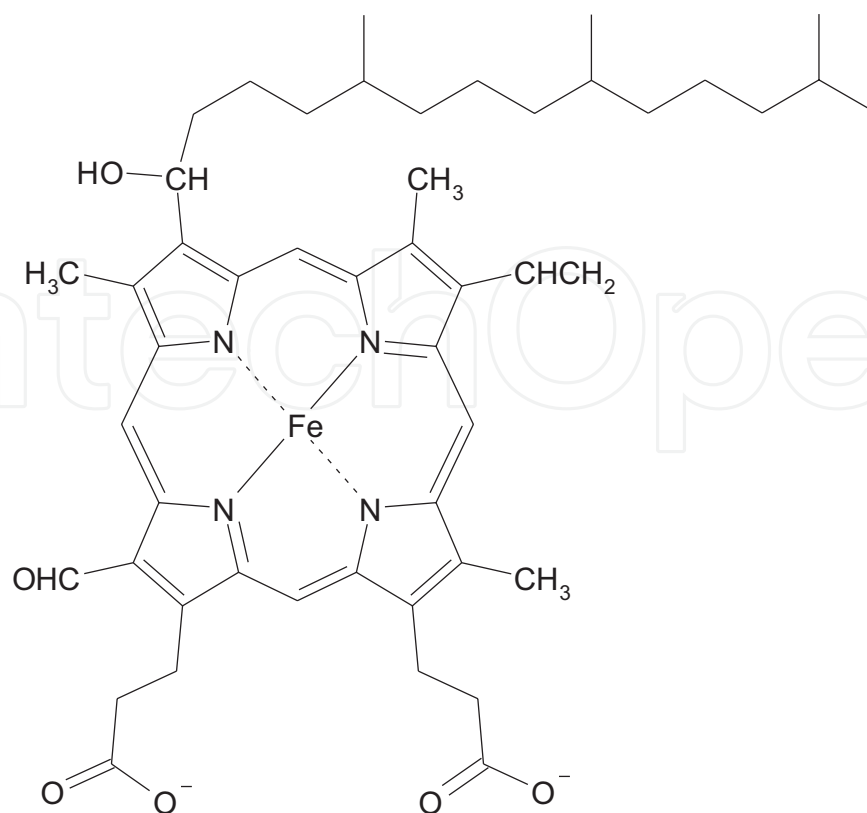
Figure 1. The structure of *haem* a.

The four polypeptide chains are bound to each other by salt bridges, hydrogen bonds, and hydrophobic interaction. While Hb does not function physiologically as an electron transfer carrier, it does undergo oxidation and reduction at the *haem* group in certain cases *in vivo* [2]. Therefore, the focused research on its electron transfer process might lead to a more profound understanding of electron flow in biological systems.

Throughout almost half of the century, there has been shown that the direct electrochemistry of *haem* proteins on bare electrodes is fairly difficult [3]. Arrival to this conclusion may be caused by several factors that were overcame to progress, among them: (a) the extended three-dimensional protein conformation due to strong interaction between the protein and the substrate or the lack of an effective microenvironment for adsorption; (b) the inaccessibility of electron communication between the electroactive center of the protein and the electrode due to misalignment of the redox center of the protein; (c) the adsorption of denatured protein onto electrodes, resulting in a loss of bioactivity; and (d) the unsymmetrical distribution of surface charges on protein molecules. According to point (c), a general problem commonly found with used metal electrodes, such as Au, Ag, Pt, and Hg, is that all of them lead to denaturation and irreversible adsorption of the resulting inactive protein, and they are easily fouled by contaminants, i.e., the water molecules that are normally bound at the electrode/electrolyte interface are easily displaced (*cf.* **Figure 2**).

Since the pioneering studies of Rusling and co-workers [4, 5] in the 1990s, the most successful electrode materials for *haem* proteins have been carbon or metal oxides, which bear well-defined natural surface functionalities. Semiconducting metal oxides are often optically
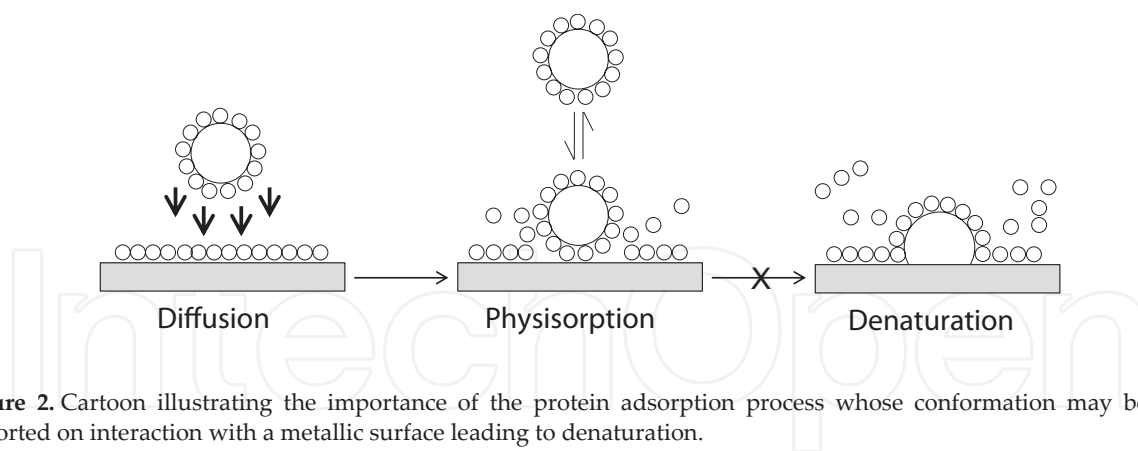
Figure 2. Cartoon illustrating the importance of the protein adsorption process whose conformation may become distorted on interaction with a metallic surface leading to denaturation.

transparent across the visible spectrum and thus provide additional possibilities for spectral studies, e.g., fluorescence and Raman spectroscopies. In the last decade, a few studies have been conducted on mammalian's Hb, for example, Topoglidis et al. [6] reported that tita-nium oxide and tin oxide allow the reduction of bovine metHb without the addition of any promoters and mediators. Later, Ayato et al. [7, 8] reported that tin-doped indium oxide can induce the electron transfer of the *haem* (Fe^{III}/Fe^{II}) redox center in bovine Hb molecules; they also found that the protein directly adsorbed on the electrode surface was not significantly denatured. More recently, Martinez-Mancera and Hernandez-Lopez [9] reported that thin films of solid solutions like $In_{2-x}Sn_xO_3$ on flat glass substrates can act as both electron acceptors and electron donors, and can be considered a simple model system for mimicking a charge interface of the physiological-binding domain. Herein, the electron transfer properties of the *haem* (Fe^{III}/Fe^{II}) redox center in human Hb molecules were investigated, *in vitro*, on commer-cial glass/tin-doped indium oxide (ITO) electrodes. Special emphasis is put in theory of cyclic voltammetry and in the Butler-Volmer model, developed by Laviron, for studying the elec-tron transfer between electrode and protein film, the morphological, structural, and surface properties of the electrode, as well as the influence of the physiological milieu that was con-ditioned into the three-electrode cell system by means of a phosphate-buffered saline (PBS) solution (0.01 mol L^{-1} Na_3PO_4, 0.015 mol L^{-1} NaCl, pH 7.2) and $T = 25°C$. To this chapter, we have added supplementary information. Subsection 2.2.1. A procedure of chromatography in-column, which underlines the importance of preparing and purifying the protein solution. Subsection 2.6. A model of theoretical prediction for determining the point of zero charge of the working electrode.

2. Experimental

2.1. Chemicals

Human hemoglobin (Product No. H7379, pH_{iep} = 6.87, MW = 64.5 kDa) and phosphate-buffered saline (PBS) packs (0.01 mol L^{-1} Na_3PO_4, 0.015 mol L^{-1} NaCl, pH 7.2), BupH™ were purchased from Sigma-Aldrich® and Thermo Scientific®, respectively, and used without further purifica-tion. Sodium dithionite ($Na_2S_2O_4$), FW = 174.110 g mol^{-1} was purchased from J.T. Baker and used

without further purification. BACKBOND spe™, Sephadex® G-25, disposable extraction columns were purchased from J.T. Baker. The concentration of Hb was adjusted to 1×10^{-4} mol Hb L^{-1} using the PBS solution.

2.2. Characterization of the protein by UV-visible spectroscopy

Absorption spectra of human Hb were measured at λ = 200–1000 nm with an UV-Visible spectrophotometer 101 GBS (*Cintra*), using the following parameters: step size = 0.16 nm, scan speed = 400 nm/min, slit width (SW) = 2 nm. The concentration of Hb referred above was estimated by this technique using the following absorptivity value: A_{540} (1%) = 5.97 cm^{-1} [10] (*cf.* **Figure 3**).

2.2.1. Preparation of reduced hemoglobin from oxidized hemoglobin

Reduced hemoglobin can be prepared from oxidized hemoglobin in accordance to the work reported by Dixon and McIntosh [11] with modifications. Briefly, the procedure is as follows: (a) equilibrate a column of Sephadex G-25 (25 × 2.5 cm) with a 20×10^{-3} mol L^{-1} PBS solution, pH 7.0, containing 1×10^{-3} mol L^{-1} EDTA; (b) apply to the column 2 mL of the same buffer to which 1×10^{-3} mol of Na$_2$S$_2$O$_4$ have been added, and help it drain into the gel by adding 1 mL of the PBS solution; (c) apply to the column about 10 mL of sample containing oxidized hemoglobin and elute with the PBS solution; (d) saturate the reduced hemoglobin eluent with oxygen gas; and (e) dialyze the oxygenated eluent against an oxygen-saturated PBS solution in order to eliminate any excess of S$_2$O$_4{}^{2-}$ and achieve complete conversion to oxyhemoglobin.
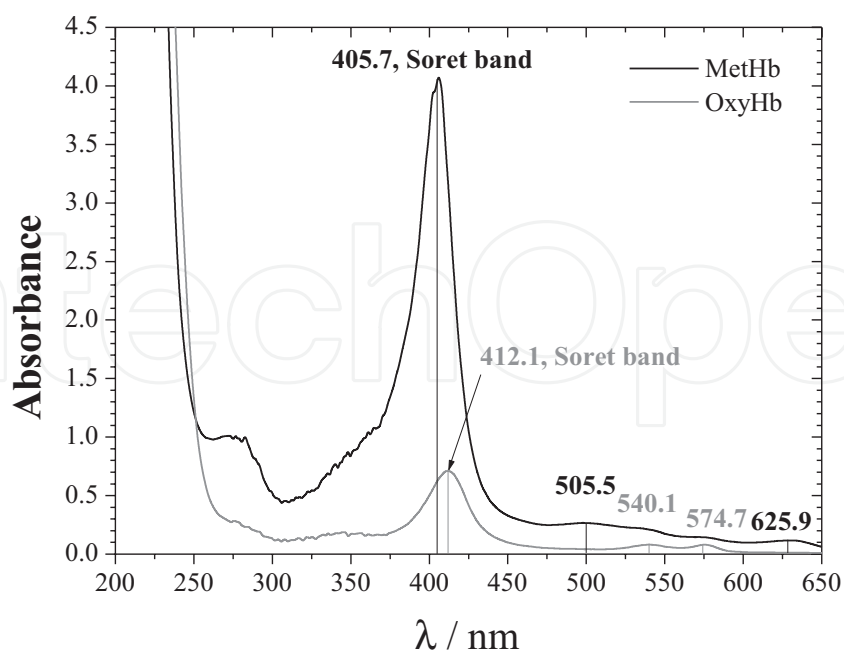

Figure 3. The UV-visible absorption spectra for metHb and oxyHb exhibiting the highly conjugated porphyrin macrocycle with intense features at 405.7 and 412.1 nm (the "Soret" bands), respectively, followed by several weaker absorptions (Q bands) at higher wavelengths (from 450 to 650 nm) [12–14].

2.3. Electrochemical measurement system

Glass/tin-doped indium oxide (ITO) substrates were purchased from *TIRF Technologies, Inc*. The ITO film surface was cleaned according to the following standard procedure [15]: immersion for 15 min each in a series of ultrasonically agitated solvents (acetone, ethanol, water) then for 15 min each in ultrasonically agitated: (a) 2.0% (v/v) phosphate-free detergent solution Hellmanex (*Hellma*™; sonification apparatus Super RK510, *Sonorex*), (b) deionized water type I and (c) ethanol at room temperature. In between the sonification steps, the samples were rinsed in deionized water type I. Finally, the substrates were dried in a stream of nitrogen gas (*Praxair*, 99.999%) until further processing. The electrode potential was controlled with a potentiostat-galvanostat EW-4960 (*Epsilon*™ *BASi*) using a conventional three-electrode cell system supported onto a module C3 (*BASi*). The latter is coupled to a PC/Processor Intel® Celeron, 3.06 GHz. A glass/ITO substrate (A_g = 1.15 cm²) was used as working electrode. A straight platinum wire (A_g = 0.79 mm²) and an electrode of Ag|AgCl in 3 M NaCl solution ($E^{0'}$ = 0.209 V vs. SHE at 25°C) were used as counter and reference electrodes, respectively. The cell system was thermostated at 25 ± 0.1°C. Prior to voltammetry, the Hb solution was purged with nitrogen gas (*Praxair*, 99.999%) for at least 30 minutes; then, a nitrogen atmosphere was maintained over the solution during experiments.

2.4. SEM and surface roughness analysis

Scanning electron microscopy (SEM) micrographs were taken with a scanning electron microscope JSM-6510LV (*JEOL*) operated at an accelerating voltage of 15 KV. The superficial characterization of the electrode's roughness was carried out by means of a surface roughness tester HANDYSURF E-35A (*TSK/Carl Zeiss®*) and performing the norm ASME B46.1-2009 Standard.

2.5. XRD analysis

The structural characterization was determined by X-ray powder diffraction (XRD) using a diffractometer D8 Advanced (*Bruker AXS*), using the following parameters: *U* = 40 kV, *I* = 35 mA, Ni-filter, and Cu-Kα radiation, λ = 1.54 Å. A background diffractogram was subtracted using a glass/tin-doped indium oxide slide as blank. For qualitative analysis, XRD diffractograms were recorded in the interval 10° ≤ 2θ ≥ 80° at a scan speed of 2°/min.

2.6. Theoretical prediction of the point of zero charge of a glass/ITO electrode

The point of zero charge (PZC) of simple metal oxides can be predicted using an electrostatic model, which takes into account the surface charges originating from the dissociation of amphoteric surface M–OH groups and adsorption of the hydrolysis products of $M^{z+}(OH)^{z-}$ [16]. In this model, a theoretical value of the PZC can be obtained for a given metal oxide by the following equation

$$pH_{pzc} = A - 11.5\left[\frac{z}{R} + 0.0029(\text{CFSE}) + B\right] \tag{1}$$

with

$$R = 2r_O + r_M \tag{2}$$

where z is the ionic charge of species indicated by the subscript, i.e., O = O_2^- and M = cation, r is the ionic radius (r_O = 0.141 nm, r_M = 0.071 nm and 0.081 nm for Sn^{4+} and In^{3+}, respectively), CFSE is a correction factor called crystal field stabilization energy and the constants A and B are parameters that depend on the coordination number of the cation. By virtue of that Sn^{4+} and In^{3+} occupy octahedral interstitial sites in SnO_2 and In_2O_3, the coordination number for these ionic species is 6. Assuming that CFSE is zero in these calculations, A = 18.6 and B = 0 [16]. The predicted PZC values obtained for SnO_2 and In_2O_3 are then $pH_{pzc}(SnO_2)$ = 5.93 and $pH_{pzc}(In_2O_3)$ = 9.37 [16].

For solid solutions such as ITO, the pH_{pzc} can be considered as a mixture of the constitutive simple oxides and can be calculated by the following equation [17]

$$pH_{pzc} = \Sigma_k s_k\, pH_{pzc,k} \tag{3}$$

where s_k represents the molar fraction of each constituting oxide at the surface. It can be defined by

$$s_k = \frac{x_k^{2/3}}{\sum_k x_k^{2/3}} \tag{4}$$

where x_k is the usual volumetric molar fraction of each constituting oxide.

3. Results and discussion

3.1. Morphological, structural, and electrochemical characterization of a glass/ITO electrode

3.1.1. Morphological and surface roughness analysis

The surface morphology of a pretreated glass/ITO electrode was investigated using SEM (*cf.* **Figure 4**). The micrograph, taken at a 500 μm scale, shows a layer of ITO well defined whose thickness was *ca.* 90 μm. Besides, it is possible to observe a regular, uniform, and flat electrodic surface.

Additionally, the average roughness value obtained in this case was 0.017 μm, which is comparatively lower than the average roughness value obtained for a common glass slide (0.024 μm).

3.1.2. Structural analysis

The structural characterization of a pretreated glass/ITO electrode was investigated using XRD. **Figure 5** shows the XRD pattern of a glass/ITO substrate used like a working electrode. All of the distinct diffraction peaks corresponded to the (211), (222), (400), (440), and (622) reflections of the BCC structure of ITO ($In_{1.94}Sn_{0.06}O_3$) (JCPDS Card File No. 89-4596). Almost all the peaks were very prominent and referred to the cubic rock salt structure of a very crystalline material. Moreover, strong (222) and (400) diffraction peaks are indicative of preferred orientations along the ⟨111⟩ and ⟨100⟩ directions, respectively [18].
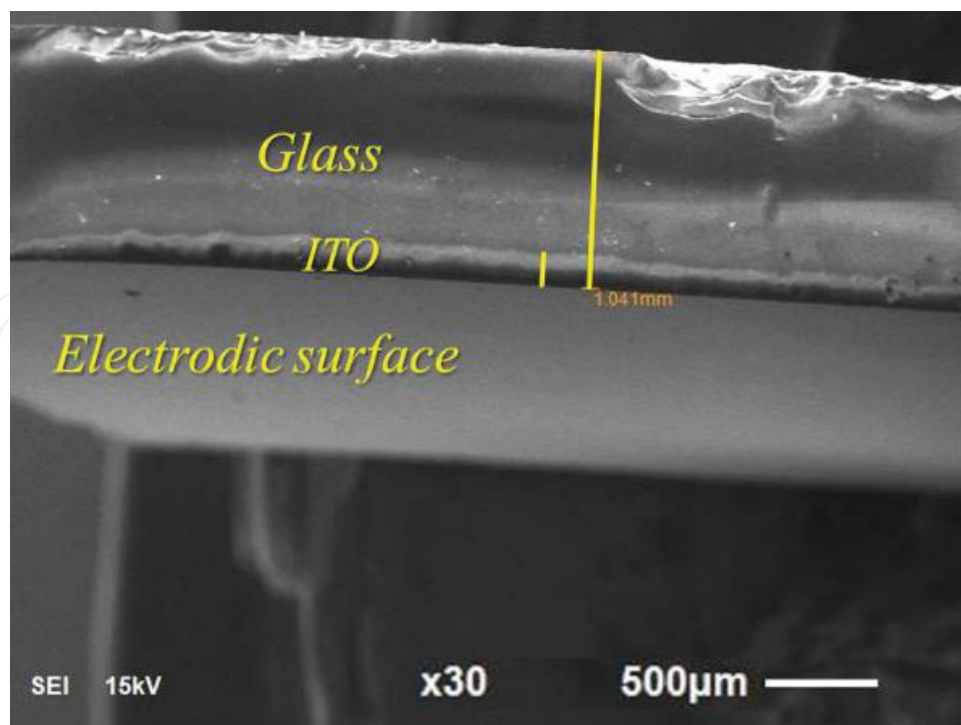
Figure 4. Cross-sectional SEM micrograph of a glass/ITO electrode.
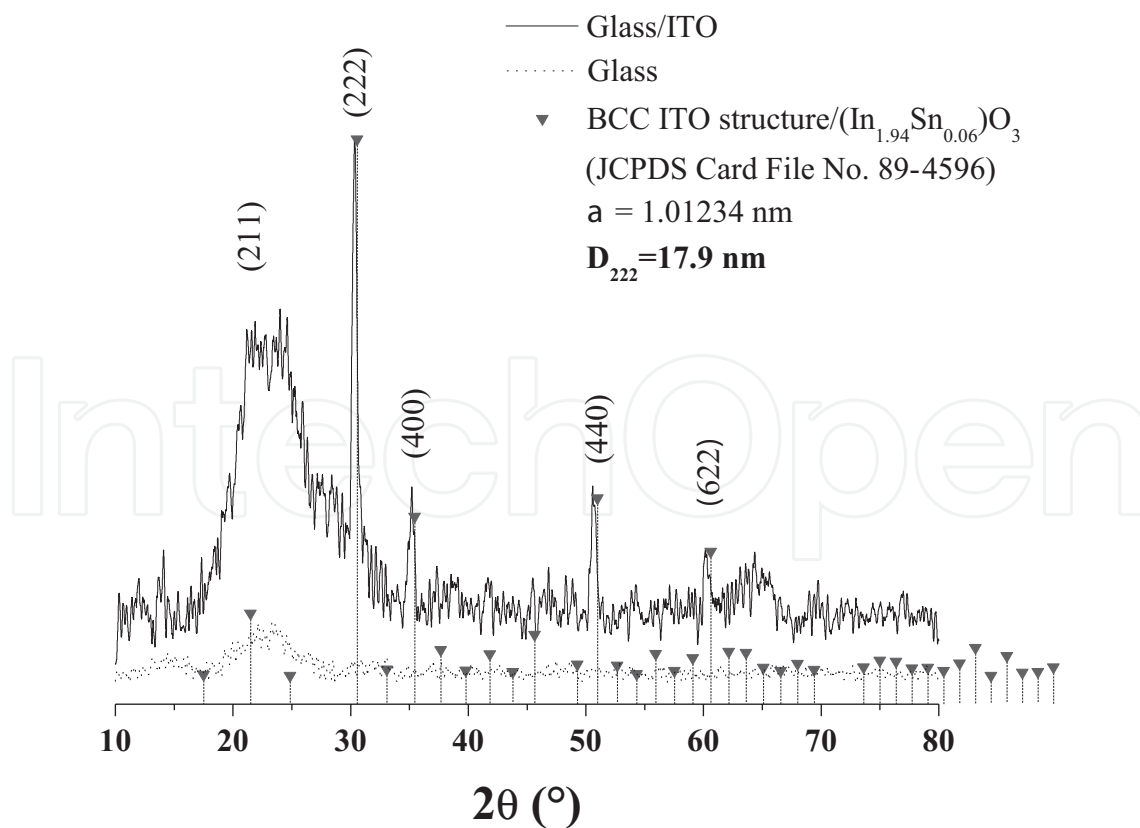

Figure 5. X-ray diffraction pattern of a glass/ITO electrode.

An estimate of the mean crystallite or grain size for a given orientation was determined by using Scherrer's formula [19]:

$$D_{hkl} = \frac{K\lambda}{\beta_{hkl}\cos\theta} \tag{5}$$

where D_{hkl} is the crystallite size (nm), K is a constant (shape factor, about 0.90), λ is the X-ray wavelength (1.54 Å as mentioned before), $\beta_{hkl} = \Delta(2\theta)$ denotes the full width at half maximum (FWHM) or broadening of the diffraction peak (degree), and θ is the diffraction angle (degree). The average D_{hkl} was estimated to be approximately $D_{222} = 17.9$ nm for $2\theta = 30.566°$. It is worth mentioning that the calculated lattice constant a for the glass/ITO substrate using Bragg's equation was $a = 1.01234$ nm, which coincides with the reported value in the standard card.

3.1.3. Electroactive surface area determination

By measuring the peak current in cyclic voltammograms (CVs), the electroactive surface area of a pretreated glass/ITO electrode was determined according to the Randles-Ševčik equation for a reversible electrochemical process under diffusive control:

$$I_{pa} = 0.4463nF\, A_e C_{OX}\sqrt{\frac{nFvD}{RT}} \tag{6}$$

where I_{pa} is the anodic peak current (A), n is the number of electrons transferred in the redox reaction, F is Faraday's constant (96,485 C mol^{-1} of electrons), A_e is the electroactive surface area of the electrode (cm^2), C_{OX} is the bulk concentration of an oxidant molecule in the solution (mol cm^{-3}), v is the scan rate (V s^{-1}), D is the diffusion coefficient of the oxidant molecule in solution, $(6.50 \pm 0.02) \times 10^{-6}$ cm^2 s^{-1}, for hexacyanoferrate (II) in 0.1 mol L^{-1} KCl as supporting electrolyte at 25°C [20], R is the gas universal constant (8.314 J K^{-1} mol^{-1}), and T is the absolute temperature (K).

CVs for 4.0×10^{-3} mol L^{-1} hexacyanoferrate (II) in 0.1 mol L^{-1} KCl were registered to different scan rates ($v = 10, 20, 30, 40, 50, 60, 70, 80, 90$, and 100 mV s^{-1}) with the glass/ITO electrode. The peak-to-peak potential separation was constant and linear relationships between the anodic and cathodic peak currents and the square root of the scan rate: $I_{pa} = 0.00101v^{1/2} - 5.8550 \times 10^{-7}$, $R^2 = 0.9999$; $- I_{pc} = 0.00101v^{1/2} + 3.2078 \times 10^{-7}$, $R^2 = 0.9999$, were achieved. From the slope of these equations, A_e was calculated to be 1.36 cm^2. The roughness factor (ρ) of the GME, which is defined as the ratio (A_e/A_g) [21], was estimated to be 1.18.

3.2. Electrochemical behavior of human hemoglobin molecules

The most popular methods for studying redox enzyme or protein electrochemistry are those based on controlled potential techniques: linear sweep voltammetry (LSV), square wave voltammetry (SWV), and cyclic voltammetry (CV). In the latter, the scan rate, defined as $v = \Delta E/\Delta t$, can be varied from less than 1×10^{-3} V s^{-1} to 1×10^{6} V s^{-1} or more, offering a practical timescale window from minutes to microseconds, which makes to this technique very suitable to study interfacial electron transfer kinetics.

Consider the following hypothetical reversible electrochemical reaction: Ox + ne− $\rightleftharpoons$ Red, the interconversion given between oxidized (Ox) and reduced (Red) forms of the protein are fast

on the timescale of the voltammogram, as controlled by scan rate. Ideal, reversible voltammograms from a monolayer of electroactive protein on an electrode for a simple electron transfer reaction as it was written above are similar to those of any ultrathin electroactive film. A protein-film voltammetry approach is described in more detail in the following section of this chapter.

3.2.1. Cyclic voltammetry of thin protein films

Figure 6 shows the CVs of glass/ITO electrodes in absence and presence of Hb molecules. In **Figure 6a**, a CV recorded in PBS solution alone shows a non-Faradaic current behavior. The electrode had the largest background current in the nonelectrolyte solution which reflected the properties of the electric double layer. The double layer capacitance (C_{dl}) can be estimated by dividing the sum of the anodic and cathodic current with twice the scan rate, i.e., $C_{dl} = (I_{pa} + I_{pc})/2v$ [21]. So, the capacitances of the glass/ITO and glass/ITO/Hb electrodes were calculated from **Figure 6a** and **b** as 4.8 and 0.4 $\mu F\ cm^{-2}$, respectively. In **Figure 6b**, a pair of redox peaks, at around −0.117 V in the cathodic scan and at around −0.097 V in the anodic scan, were found in that Hb-containing solution. This fact indicated that a Faradic current was generated over the glass/ITO electrode, which can be adscribed to the *haem* (Fe^{III}/Fe^{II}) redox center in Hb molecules.

Once capacitive effects are counted out, the amount of electrochemically active Hb molecules could be estimated from integration of the charge Q (in C) under each peak in those CVs acquired at slow scan rates (i.e., 0.1, 0.3, or 0.5 V s^{-1}), given by Faraday's law:

$$Q = nFA_e\Gamma_T \tag{7}$$

where Γ_T is total surface concentration of the protein molecule (mol cm^{-2}), A_e is the electroactive surface area of electrode (cm^2), F is Faraday's constant (96,485 C mol^{-1} of electrons) and n is the number of electrons transferred in the redox reaction:
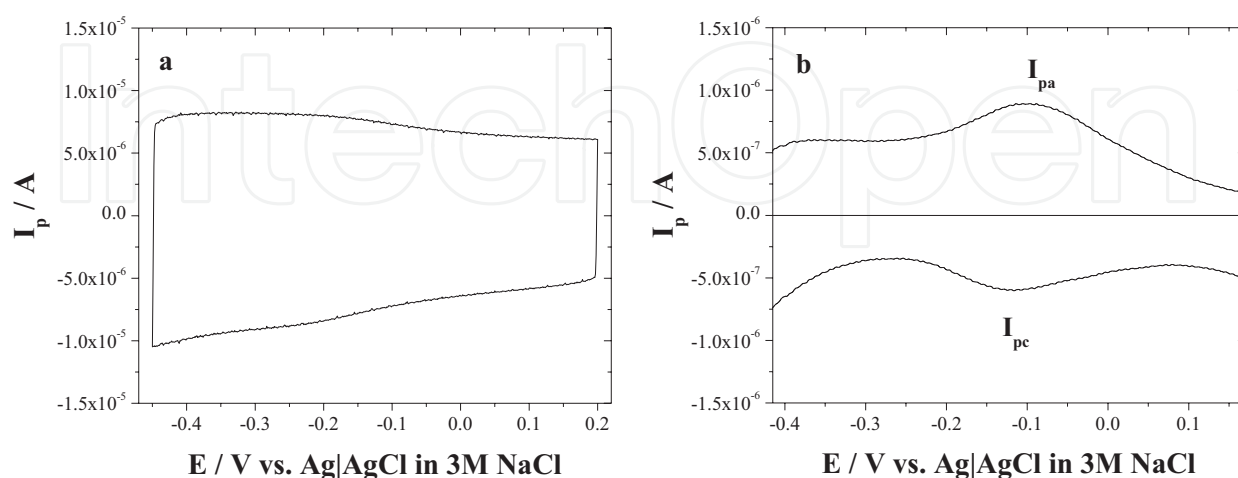
$$Hb:\ haem(Fe^{III}) + H_3O^+ + e^- \rightarrow haem(Fe^{III}) \tag{8}$$

Figure 6. (a) Cyclic voltammograms of: (a) a PBS solution (0.01 mol L^{-1} Na_3PO_4, 0.015 mol L^{-1} NaCl, pH 7.2) and (b) a PBS solution (0.01 mol L^{-1} Na_3PO_4, 0.015 mol L^{-1} NaCl, pH 7.2) containing 1.0 × 10^{-4} mol human Hb L^{-1} after subtraction of (a), as a blank. The experiment was carried out at T = 25°C. Scan rate: 0.5 V s^{-1}.

The total surface concentration of electroactive Hb molecules was estimated to be Γ_T = (4.69 ± 0.52) × 10^{-12} mol cm^{-2}. On the other hand, the theoretical maximum coverage of a protein monolayer on the electrode surface was estimated as 4.89 × 10^{-12} mol cm^{-2}, considering that one human Hb molecule in PBS solution has a Stokes radius of 31.3 Å [22]. These data indicate that $\theta = (\Gamma_T/\Gamma_{T,theo})$ = 0.96 of a protein monolayer was achieved.

Figure 7a shows CVs recorded with different scan rates, from 0.1 to 3.5 V s^{-1}. Nearly symmetric anodic and cathodic peaks were observed; in addition, they have roughly equal heights. The anodic to the cathodic peak potential difference (ΔE_p) was much greater than the ideal value of zero. At the lower scan rates, i.e., 0.1, 0.3, or 0.5 V s^{-1}, the smaller redox peak currents were observed, while CVs with the largest redox peak currents corresponded to those acquired at the fastest scan rate, i.e., 3.5 V s^{-1}.

In such cases, the formal potential $E^{0\prime}$ was taken as the midpoint potential between the oxidation and reduction peaks if there is a small separation between them. Considering this criterium, an $E^{0\prime}$ = −0.107 V (vs. Ag|AgCl in 3 M NaCl solution) was determined at 0.5 V s^{-1}. On the other hand, the anodic and cathodic peak currents, I_{pa} and I_{pc}, increased with increasing scan rates as observed in **Figure 7b**.

These results are characteristic of quasireversible, surface confined electrochemical behavior, in which all electroactive proteins in their *haem* (Fe^{III}) forms are reduced on the forward cathodic scan, and the reduced proteins in their *haem* (Fe^{II}) forms are then fully oxidized to the *haem* (Fe^{III}) forms on the reversed anodic scan.

When the peak currents were plotted against the scan rate, direct linear relationships were obtained, indicating a surface-controlled electrode process. The origin of this process is indicative that the diffusion of H$_3$O$^+$ ions toward the electrode surface was very fast. Therefore, the electron process can be expressed as proposed in the redox reaction before [23].
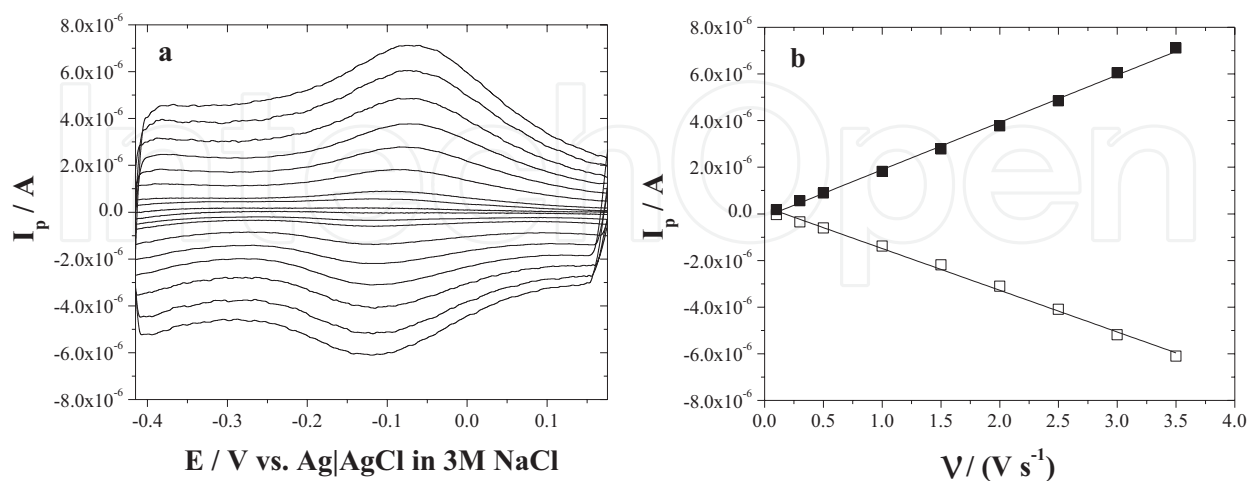

Figure 7. (a) Corrected cyclic voltammograms of a PBS solution (0.01 mol L^{-1} Na$_3$PO$_4$, 0.015 mol L^{-1} NaCl, pH 7.2) containing 1.0 × 10^{-4} mol human Hb L^{-1} (T = 25°C) as function of scan rate. Scan rates: 0.1, 0.3, 0.5, 1.0, 1.5, 2.0, 2.5, 3.0, and 3.5 V s^{-1}. (b) Dependence of anodic (■) and cathodic (□) peak currents with scan rate: I_{pa} = 2.0305 × 10^{-6}v − 1.3809 × 10^{-7}, R^2 = 0.9987; − I_{pc} = 1.7896v − 3.0310 × 10^{-7}, R^2 = 0.9985.

The linear regression equations for anodic and cathodic peak currents are as follows: $I_{pa} = 2.0305 \times 10^{-6}\nu - 1.3809 \times 10^{-7}$, $R^2 = 0.9987$; $-I_{pc} = 1.7896\nu - 3.0310 \times 10^{-7}$, $R^2 = 0.9985$.

Linear plots of I_p vs. ν were in good agreement with the following equation [24]:

$$I_p = \frac{n^2F^2A_e\Gamma_T\nu}{4RT} \quad (9)$$

However, their width at half height is nearly 200 mV, much larger than the ideal $90.6/n$ mV at 25°C.

Broadening or narrowing of CV peaks compared to the ideal $90.6/n$ mV at 25°C suggests a breakdown of the ideal model assumptions of no interactions between redox sites that all have the same $E^{0\prime}$. Representative examples arose from studying cytochrome c and myoglobin on Au/alkanethiolate SAMs and OPG/LC surfactants, respectively. Some authors have modeled protein films by LSV, SWV, and CV techniques considering the concepts of spatial distribution of the redox centers, dispersion models of formal potentials ($E^{0\prime}$), and electron transfer rate constants to account for the peak broadening [25–27]. Other factors, e.g., lack of refinement of mathematical algorithms for the extraction of rate constants or improvements to the goodness of fit of SWV data to pulse heights >50 mV, including counterion transport efficiency, could also influence peak widths, but have not been investigated in detail for protein films.

At scan rates <0.5 V s^{-1}, ΔE_p was nearly constant in the films. As the scan rate increased, the peak potentials shifted negatively (*cf.* **Figure 8**). This is consistent with the onset of limiting kinetic effects as scan rates increase.
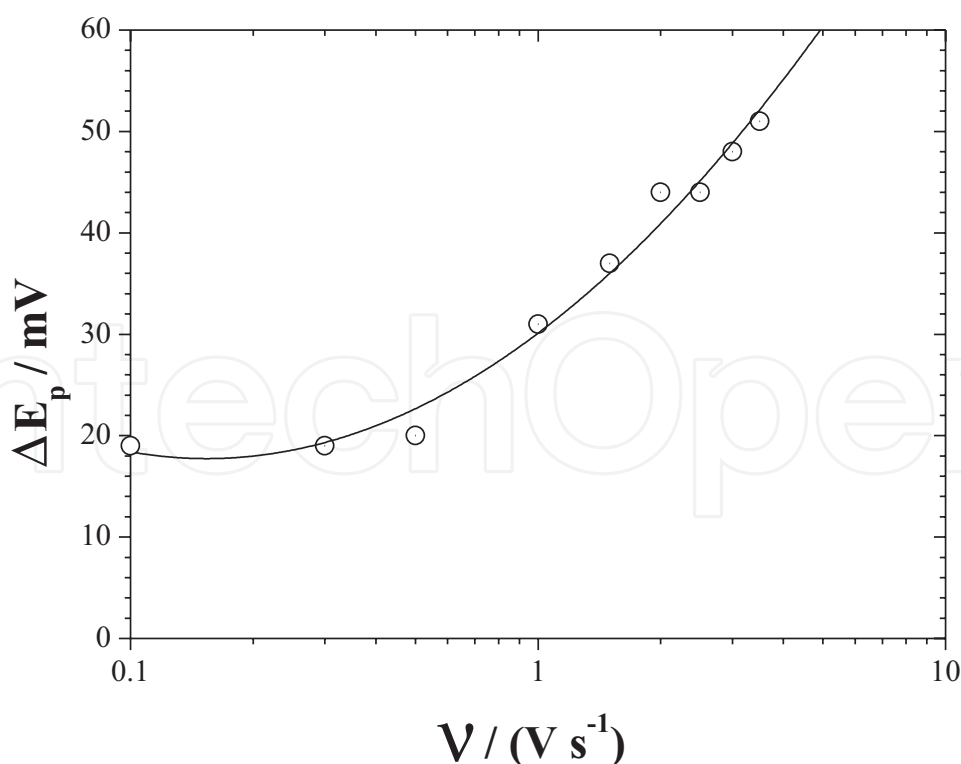

Figure 8. Influence of scan rate on the anodic to the cathodic peak potential difference (ΔE_p) for a PBS solution (0.01 mol L^{-1} Na$_3$PO$_4$, 0.015 mol L^{-1} NaCl, pH 7.2) containing 1.0×10^{-4} mol human Hb L^{-1}. The experiment was carried out at T = 25°C.

An increasing ΔE_p as the scan rate is increased for an electroactive thin film suggests kinetic limitations of the electrochemistry [28] and is consistent with predictions of the Butler-Volmer model for electron transfer between an electrode and redox sites in a thin film on an electrode. Possible causes could be attributed to: (a) slow electron transfer between electrode and redox centers, (b) slow transport of charge within the film limited by electron or counterion transport, (c) uncompensated voltage drop within the film, and (d) structural reorganization of the protein accompanying the redox reactions.

When $n\Delta E_p < 200$ mV, the surface electron transfer rate constant (k_s) of the adsorbed Hb on the glass/ITO electrode can be estimated according to Laviron's equation for quasi-reversible thin-layer electrochemistry [29]:

$$\text{Log } k_s = \alpha \text{ Log } (1 - \alpha) + (1 - \alpha) \text{ Log } \alpha - \text{Log } \frac{RT}{nFv} - \alpha(1 - \alpha) \frac{nF\Delta E_p}{2.3RT} \quad (10)$$

Our experimental results showed that the scan rate in the range 0.1–3.5 V s^{-1} did not affect the k_s value, because $n\Delta E_p < 200$ mV. Assuming a charge-transfer coefficient α of 0.5, the k_s of the adsorbed Hb thin film on the glass/ITO electrode was 8.01 s^{-1} at the onset of limiting kinetic effects (500 mV s^{-1}). This value is significantly higher than other previously reported values in the literature for different hemoglobin species and electrode materials (*cf*. **Table 1**). For comparison with data on bare or mediator-coated electrodes, k_s was converted to the standard heterogeneous rate constant ($k^{0'}$) by using $k^{0'} = k_s\ d$, where d is the film thickness [29]. This fact could be attributed to the morphological and structural properties shown by the electrode, i.e., surface roughness, crystallinity, and hydrophilicity [30], as well as the influence of the physiological milieu that was conditioned into the three-electrode cell system, charging positively/negatively to the working electrode (*cf*. Section 2.6 and Ref. [31]) and negatively to the protein [32]. All these factors played an important role in providing a more favorable microenvironment for the protein.

pH	Sample │ electrode	$E^{0'}$/mV (SHE)	$k^{0'}$/cm s^{-1}	References
5.5	[b]Hb-DDAB-Nafion │ edge-plane PG	80	5.7 d^*	[4]
5.5	[h]Hb-DDAB │ edge-plane PG	84	2.7 d^*	[5]
5.5	[h]Hb in solution │ edge-plane PG	Not detected	Not detected	op. cit. [5]
7.0	[b]Hb in solution │ Pt + MB	145	2.0×10^{-4}	op. cit. [5]
7.0	[b]Hb in solution │ Pt + Azure A	180	3.5×10^{-6}	op. cit. [5]
7.0	[b]Hb in solution │ Pt + BCG	184	2.0×10^{-7}	op. cit. [5]
7.0	[b]Hb in solution │ SnO2	−215	0.53 d^*	[6]
7.4	[b]Hb in solution │ In$_{2-x}$Sn$_x$O$_3$	−112	Not determined	[7, 8]
7.2	[h]Hb in solution │ In$_{1.94}$Sn$_{0.06}$O$_3$	102	8.01 d^*	[9]

DDAB = Didodecyldimethylammonium bromide, PG = pyrolytic graphite, MB = methylene blue, BCG = brilliant cresyl green.

*For comparison with CV data where diffusion control pertains, k_s was estimated from the standard heterogeneous rate constant ($k^{0'}$) by using $k^{0'} = k_s \cdot d$, where d is the film thickness [29].

Table 1. Electrochemical parameters for different mammalian (superscripts: b-bovine, h-human) hemoglobin species at 25°C.

As indicated in Section 1, Introduction, to facilitate the electron communication between the prosthetic group of *haem* proteins and an electrode due to misalignment of the *haem* (Fe^{III}/Fe^{II}) redox center is a difficult task but could help to advance understanding on biological electron transfer. Techniques such as FT-IR spectroscopy, NMR, ESR anisotropy, polarized reflectance FT-IR, circular dichroism, and calorimetry could yield detailed information on the secondary structure of the protein in regards to its redox state as well as to give some notion of order and specific orientation.

4. Conclusions

In this study, we clearly demonstrated that human Hb molecules directly physisorbed on glass/tin-doped indium oxide substrates exhibited direct electron transfer (DET) in PBS (0.01 mol L^{-1} Na_3PO_4, 0.015 mol L^{-1} NaCl, *pH* = 7.2) solution and T = 25°C.

The experimental results suggest that acid-base equilibria and the water molecule coordinated to the *haem* group as the sixth ligand might play an important role in the electron transfer process between human hemoglobin and very crystalline and hydrophilic tin-doped indium oxide electrodes.

Acknowledgments

Author details

Flavio Dolores Martínez-Mancera and José Luis Hernández-López*

*Address all correspondence to: jhernandez@cideteq.mx

Center of Research and Technological Development in Electrochemistry, Parque Tecnológico Querétaro S/N, Pedro Escobedo, Mexico

References

[1] Perutz MF, Wilkinson AJ, Paoli M, Dodson GG. The stereochemical mechanism of the cooperative effects in hemoglobin revisited. Annual Review of Biophysics and Biomolecular Structure. 1998;**27**:1–34. DOI: 10.1146/annurev.biophys.27.1.1

[2] Schumacher MA, Dixon MM, Kluger R, Jones RT, Brennan RG. Allosteric transition intermediates modelled by crosslinked haemoglobins. Nature. 1995;**375**(6526):84–87. DOI: 10.1038/375084a0

[3] Armstrong FA. Voltammetry of proteins. Wilson, G.S., editors. Bioelectrochemistry. Weinheim, Germany: Wiley-VCH Verlag GmbH; 2002. pp. 11–29

[4] Huang Q, Lu Z, Rusling JF. Composite films of surfactants, nafion, and proteins with electrochemical and enzyme activity. Langmuir. 1996;**12**(22):5472–5480. DOI: 10.1021/la9603784

[5] Lu Z, Huang Q, Rusling JF. Films of hemoglobin and didodecyldimethylammonium bromide with enhanced electron transfer rates. Journal of Electroanalytical Chemistry. 1997;**423**(1–2):59–66. DOI: 10.1016/S0022-0728(96)04843-7

[6] Topoglidis E, Astuti Y, Duriaux F, Grätzel M, Durrant JR. Direct electrochemistry and nitric oxide interaction of heme proteins adsorbed on nanocrystalline tin oxide electrodes. Langmuir. 2003;**19**(17):6894–6900. DOI: 10.1021/la034466h

[7] Ayato Y, Itahashi T, Matsuda N. Direct electron transfer of hemoglobin molecules on bare ITO electrodes. Chemistry Letters. 2007;**36**(3):406–407. DOI: 10.1246/cl.2007.406

[8] Ayato Y, Takaktsu A, Kato K. Matsuda, N. Direct electrochemistry of hemoglobin molecules adsorbed on bare indium tin oxide electrode surfaces. Japanese Journal of Applied Physics. 2008;**47**(2S):1333–1336. DOI: 10.1143/JJAP.47.1333

[9] Martínez-Mancera FD, Hernández-López JL. In vitro observation of direct electron transfer of human haemoglobin molecules on glass/tin-doped indium oxide electrodes. Journal of the Mexican Chemical Society. 2015;**59**(4):302–307

[10] Li T-K, Johnson BP. Optically active heme bands of hemoglobin and methemoglobin derivatives. Correlation with absorption and magnetic properties. Biochemistry. 1969;**8**(9):3638–3643. DOI: 10.1021/bi00837a021

[11] Dixon HBF, McIntosh R. Reduction of methaemoglobin in haemoglobin samples using gel filtration for continuous removal of reaction products. Nature. 1967;**213**(5074):399–400. DOI: 10.1038/213399a0

[12] Smith KM., editors. Porphyrins and Metalloporphyrins. Amsterdam, The Netherlands: Elsevier; 1975. p. 910

[13] Boulton M, Rozanowska M, Rozanowski B. Retinal photodamage. Journal of Photochemistry and Photobiology B: Biology. 2001;**64**(2–3):144–161. DOI: 10.1016/S1011-1344(01)00227-5

[14] Sagun EI, Zenkevich EI, Knyukshto VN, Shulga AM, Starukhin DA, Borczyskowski CV. Interaction of multiporphyrin systems with molecular oxygen in liquid solutions: Extra-ligation and screening effects. Chemical Physics. 2002;**275**(1–3):211–230. DOI: 10.1016/S0301-0104(01)00517-1

[15] Hernandez-Lopez JL. Water-soluble dendrimers: A novel hierarchical concept for the preparation and study of supramolecular interface based films [dissertation]. Mainz,

Germany: Fachbereich Chemie und Pharmazie der Johannes Gutenberg-Universität; 2003. p. 297

[16] Parks GA. The isoelectric points of solid oxides, solid hydroxides, and aqueous hydroxo complex systems. Chemical Reviews. 1965;**65**(2):177–198. DOI: 10.1021/cr60234a002

[17] Carre A, Roger F, Varinot C. Study of acid/base properties of oxide, oxide glass, and glass-ceramic surfaces. Journal of Colloid Interface Science. 1992;**154**(1):174–183. DOI: 10.1016/0021-9797(92)90090-9

[18] Meng L-J, dos Santos MP. Properties of indium tin oxide films prepared by rf reactive magnetron sputtering at different substrate temperature. Thin Solid Films. 1998;**322**(1–2):56–62. DOI: 10.1016/S0040-6090(97)00939-5

[19] Cullity BD. Elements of X-ray Diffraction. 2nd ed. Massachusetts, USA: Addison-Wesley, Publishing Company; 1978. p. 569

[20] Stackelberg MV, Pilgram M, Toome V. Bestimmung von Diffusionskoeffizienten einiger Ionen in wäßriger Lösung in Gegenwart von Fremdelektrolyten. I. Berichte der Bunsengesellschaft für Physikalische Chemie. 1953;**57**(5):342–350. DOI: 10.1002/bbpc.195300073

[21] Bard AJ, Faulkner LR. Electrochemical Methods: Fundamentals and Applications. 2nd ed. New York, USA: John Wiley & Sons, Inc.; 2001. p. 850

[22] Gros G. Concentration dependence of the self-diffusion of human and Lumbricus terrestris hemoglobin. Biophysical Journal. 1978;**22**(3):453–468. DOI: 10.1016/S0006-3495(78)85499-X

[23] Wang C, Yang C, Song Y, Gao W, Xia X. Adsorption and direct electron transfer from hemoglobin into a three-dimensional ordered macroporous gold film. Advanced Functional Materials. 2005;**15**(8):1267–1275. DOI: 10.1002/adfm.200500048

[24] Rusling JF, Zhang Z. Thin films on electrodes for direct protein electron transfer. In: Nalwa, R.W., editors. Handbook of Surfaces and Interfaces of Materials. San Diego, USA: Academic Press, Inc.; 2001. pp. 33–71. DOI: 10.1016/B978-012513910-6/50059-1

[25] Nahir TM, Clark RA, Bowden EF. Linear-sweep voltammetry of irreversible electron transfer in surface-confined species using the Marcus theory. Analytical Chemistry. 1994;**66**(15):2595–2598. DOI: 10.1021/ac00087a027

[26] Zhang Z, Rusling JF. Electron transfer between myoglobin and electrodes in thin films of phosphatidylcholines and dihexadecylphosphate. Biophysical Chemistry. 1997;**63**(2–3):133–146. DOI: 10.1016/S0301-4622(96)02216-8

[27] Nassar A-EF, Zhang Z, Hu N, Rusling JF, Kumosinski TF. Proton-coupled electron transfer from electrodes to myoglobin in ordered biomembrane-like films. The Journal of Physical Chemistry B. 1997;**101**(12):2224–2231. DOI: 10.1021/jp962896t

[28] Murray RW. Chemically modified electrodes. In: Bard, A.J., editors. Electroanalytical Chemistry. New York, USA: Marcel Dekker, Inc.; 1984. pp. 191–368

[29] Laviron E. General expression of the linear potential sweep voltammogram in the case of diffusionless electrochemical systems. Journal of Electroanalytical Chemistry and Interfacial Electrochemistry. 1979;**101**(1):19–28. DOI: 10.1016/S0022-0728(79)80075-3

[30] Li C-Z, Liu G, Prabhulkar S. Comparison of kinetics of hemoglobin electron transfer in solution and immobilized on electrode surface. American Journal of Biomedical Sciences. 2009;**1**(4):303–311. DOI: 10.5099/aj090400303

[31] Lin X-Y, Farhi E, Arribart H. Determination of the isoelectric point of planar oxide surfaces by a particle adhesion method. The Journal of Adhesion. 1995;**51**(1–4):181–189. DOI: 10.1080/00218469508009997

[32] Conway-Jacobs A, Lewin LM. Isoelectric focusing in acrylamide gels: Use of amphoteric dyes as internal markers for determination of isoelectric points. Analytical Biochemistry. 1971;**43**(2):394–400. DOI: 10.1016/0003-2697(71)90269-7